Quaternary International 388 (2015) 218–231

Contents lists available at ScienceDirect

Quaternary International

journal homepage: www.elsevier.com/locate/quaint

The last and penultimate glaciation in the North Alpine Foreland: New stratigraphical and chronological data from the Salzach glacier

Bernhard C. Salcher [a, *], Reinhard Starnberger [b], Joachim Götz [a]

[a] Department of Geography and Geology, University of Salzburg, Hellbrunner Strasse 34, 5020 Salzburg, Austria
[b] Institute for Geology and Palaeontology, Leopold-Franzens University of Innsbruck, Innrain 52, 6020 Innsbruck, Austria

Keywords:
Stratigraphy
Lithofacies
Luminescence dating
North Alpine Foreland
Glacier lobe
Glaciofluvial sediments

A B S T R A C T

The Northern Alpine Foreland was repeatedly covered by massive piedmont glaciers during Quaternary glacial maxima. The Salzach palaeoglacier lobe (Austria/Germany) was the easternmost of a series of Pleistocene piedmont glaciers entering the foreland through major alpine valleys. It covered an area of more than 1000 km^2 during at least four glacial maxima. Here we aim to bring more light into its history by analyzing multiple drill log data, two major outcrops, topographic data, and absolute chronologies of sediments. Stratigraphic and lithofacies investigations are focused on proximal (i.e. near the lobe axis) and distal (i.e. near terminal moraine) deposits of the Salzach glacier lobe. The glacial carving into the Miocene bedrock occurred during early glacial maxima and was rather uniform across the lobe with larger values only in the proximal parts of the glacier. More than 100 m of accumulated sediments during later glacial maxima indicate a change in ice-sheet dynamics and a characteristic sequence development which varies from proximal to distal lobe positions. New luminescence ages suggest a depositional focus at the penultimate glacial period while the impact of the LGM was rather minor. Sediments of gravelly braided-rivers dominate the proximal parts of the former lobe where meltwater discharge was generally high, while sheetflood deposits dominate the distal, near terminal lobe positions.

1. Introduction

The Alpine Foreland gives a clear impression that the large piedmont glaciers of the Quaternary were not only highly efficient erosive agents but did also leave major glacial and glaciofluvial deposits around the circum alpine realm. The tremendous impact of Quaternary glaciers on the morphology of the North Alpine Foreland was already described by Penck and Brückner (1909) more than 100 years ago and has strongly contributed to the understanding of the dynamics of major ice-lobes. The authors showed that the major ice-lobes entering the foreland left landforms associations characteristically varying from the marginal to the proximal and often overdeepened glacier lobe parts ("glacial series"). While some complexity has been added to this morphostratigraphic view (e.g. Lüthgens and Böse, 2012) it has principally been confirmed in numerous studies inside, but also outside the circum alpine realm (e.g. Eyles et al., 1999; Carlson et al., 2005; Jennings, 2006; Salcher et al., 2010). Precise digital elevation models underpinned the landform succession from ice marginal deposits to ice wastage and streamlined bed forms at the inner, proximal part of the former lobe (Carlson et al., 2005; Jennings, 2006; Salcher et al., 2010). Deep drillings and geophysical surveys revealed the existence of local overdeepenings and the filling with glacial sediments (Van Husen, 2000; Jordan, 2010; Preusser et al., 2010; Dehnert et al., 2012; Dürst Stucki and Schlunegger, 2013).

While inner-alpine overdeepenings often have considerable depths reflecting the strong confinement of glaciers, unconstrained glacier lobes of the foreland indicate the occurrence of both, local incision but also widespread erosion below the lobe area. With the recent progress in dating techniques, overdeepenings received a broader attention, especially in regions where fillings comprise lacustrine sediments acting as paleoclimatic archives (e.g. Anselmetti et al., 2010; Dehnert et al., 2012; Starnberger et al., 2013a,b; Fiebig et al., 2014). Less attention has been paid on the erosional and depositional history of the large Piedmont glacier lobes in the Alpine Foreland, even though they are of first order importance for the destructional rearrangement of the Alpine

* Corresponding author. University of Salzburg, Department of Geography and Geology, Hellbrunnerstrasse 34, Salzburg, Austria.
E-mail addresses: bernhard.salcher@sbg.ac.at (B.C. Salcher), Reinhard.Starnberger@uibk.ac.at (R. Starnberger), joachim.gotz@sbg.ac.at (J. Götz).

http://dx.doi.org/10.1016/j.quaint.2015.09.076
1040-6182/

Molasse since the onset of basin inversion in the Late Miocene (Genser et al., 2007; Kuhlemann, 2007; Gusterhuber et al., 2012). However, knowledge on the dynamics over several full-glacial periods affecting the North Alpine Foreland after the mid-Pleistocene transition remains fragmentary. Few data across the foreland and from major Alpine overdeepenings indicate a shift from incision at the earlier full-glacial periods to rather accumulation at later glacial maxima (Preusser et al., 2010 and references therein; Dehnert et al., 2012). Coherent interpretations are generally hampered by age constraints and subsurface data which provide knowledge on the spatial variability of glacial erosion and deposition (Preusser et al., 2010). This is also true in the North Alpine Foreland with landforms and bedrock topography suggesting glacial activity during four different glacial maxima.

Here, we focus on the Salzach Glacier Lobe (SGL) in an attempt to bring more light into the dynamics of a typical north alpine glacier lobe active at successive full-glacial periods. The SGL is the easternmost of a series of large piedmont glaciers, which entered the Northern Alpine Foreland through major valleys (Fig. 1). Terminal moraines and the associated outwash plains indicate that the hydrology of this ice-sheet typically varied from the proximal lobe parts with high meltwater discharge to the distal parts where meltwater discharge is lower or highly ephemeral as indicated by small distributary systems or alluvial fans.

The aim of this paper is twofold. First, we aim to investigate the stratigraphy and lithofacies of the area covered by the SGL by analyzing driller's lithologic logs and two deep outcrops located at a proximal and a distal (ice marginal) position of the former glacier lobe. In a second step, we try to constrain the erosional and depositional variations of the Mid-to Late Pleistocene SGL by combining stratigraphic information from deep outcrops, luminescence ages and drill log data. Here we present the first luminescence ages from fluvial sediments deposited within or directly at the terminal moraines framing a North Alpine Piedmont ice-lobe. This allows us to clearly verify ages and observations using morphostratigraphic principles (e.g. Penck, 1882; Lüthgens and Böse, 2012). Very minor anthropogenic overprint of as well as comprehensive geological and topographical datasets provide a unique opportunity to investigate glacial and glaciofluvial landform associations.

2. Study area

Remnants of the SGL show the easternmost occurrence of piedmont glaciers in the Alpine Foreland. It was comparable in size and extent to the major lobes of the Inn-, Iller and Rhine glacier to the West (Fig. 1). East of the SLG, glaciers were smaller during glacial maxima and stayed within or close to the alpine front (Fig. 1). The first comprehensive Quaternary geological work about the Salzach palaeoglacier region was presented by Brückner (1886) and refined by Penck and Brückner (1909). These authors identified the remnants of three glacial maxima in the North Alpine Foreland which they morphostratigraphically integrated into their concept of “Mindel”, “Riss” and “Würm”. The correlation of the concept with marine oxygen isotope records was proposed by Raymo (1997), linking the Würm maximum cold period to MIS 2 (LGM) and suggesting the glacial maxima of Günz, Mindel and Riss as being coeval with MIS 6, 12 and 16, respectively.

The last glacial maximum extent (LGM of the SGL, Würm full-glacial period), remained within the end moraines of its penultimate glacial maximum (PGM, Riss full-glacial period), and both the LGM and the PGM were less extensive than the antepenultimate

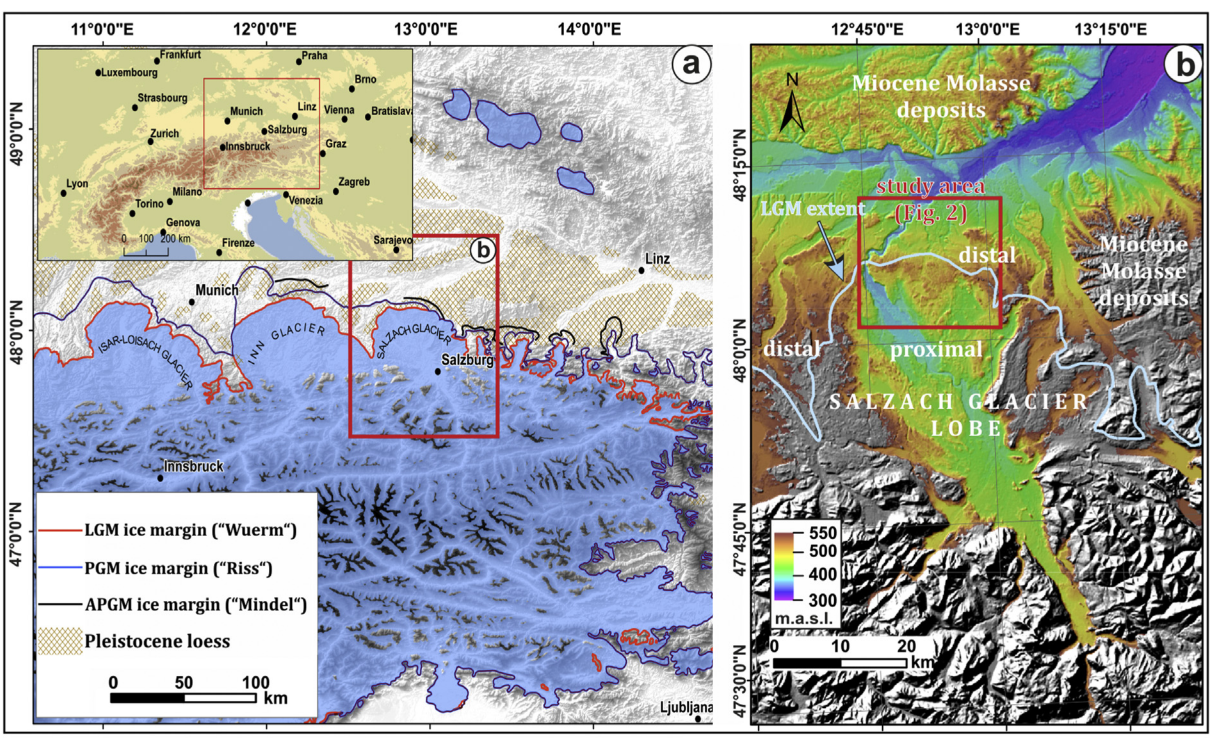

Fig. 1. Left (a): Glacier extent in the Northern Foreland of the Eastern Alps during the full-glacial periods of the last glacial maximum (LGM), the penultimate glacial maximum (PGM) and the antepenultimate maximum (APGM). The Salzach Glacier Lobe (SGL) is the easternmost of a series of piedmont lobes entering the foreland trough major Alpine valleys. Right (b): DEM showing the extension of the SGL during the LGM (blue line) and erosion into Miocene bedrock. Miocene Molasse preserved east of the major north alpine lobes. Glaciers mainly drained along the lobe axis, whereas lateral parts are rather dominated by ephemeral drainage. DEM bases on NASA's SRTM (90 m; for details see Farr and M. Kobrick, 2000). (For interpretation of the references to colour in this figure legend, the reader is referred to the web version of this article.)

glacial maximum (APGM, Mindel full-glacial period; Fig. 2). Remnants of an even older and outer terminal moraine (pre-antepenultimate glacial maximum, Günz full-glacial period) are here also preserved (Weinberger, 1950). They are generally very rare in the circum-alpine realm and are suggested to point to a slightly different ("pre-glacial") ice flow pattern at this early major glaciation (Kohl, 1998). Maximum extents of the SGL during the LGM, PGM, and APGM were very similar; spacings between former margins do not exceed 5 km (as indicated from the terminal moraines). Detailed studies on sediment–landform associations of the SGL were presented by Weinberger (1950, 1952, 1957) while Salcher et al. (2010) added more complexity to these observations by utilizing high resolution digital elevation models. Based on pollen analyses and OSL from a loess sequence, Starnberger et al. (2009, 2011) considerably contributed to the regional climatic picture around the LGM.

The glacial and glaciofluvial deposits of the SGL unconformably overly Miocene sediments resting up to about 100 m above the modern Salzach valley (Fig. 1b). The high position above the incised stream Salzach River promoted the preservation of sediments from being fluvially eroded. The situation is therefore slightly different to classical Alpine overdeepenings within the mountain belt, which act (at least to some extent) as sedimentary traps. The major alpine streams which drained the former piedmont lobes rapidly dissected sediments during and after glacial downwasting. The modern Salzach River drains about 5700 km^2 when it enters the Foreland. The dissection of up to 100 m of soft glacial and glaciofluvial sediments following deglaciation and the adaption to a quasi-equilibrium profile was likely to be completed within only a few thousands of years.

3. Material and methods

3.1. Stratigraphic assessment

Stratigraphic assessment is based on the analysis of lithofacies in three (deep) key outcrops (Fig. 2), on drill logs (~100 in total) and on luminescence dating. We furthermore adopted the concept of morphostratigraphy (e.g. Lüthgens and Böse et al., 2012) as initially introduced in the Alpine Foreland by Penck (1882).

Two outcrops are situated at the distal position of the SGL lobe, between the terminal moraines of the LGM and the PGM (Outcrop 1 and 2). The third outcrop is situated at a main drainage pathway of SGL's proximal part (Outcrop 3). Outcrops highlight sequences of diamictic, glacial and coarse-grained glaciofluvial sediments. Two of the three outcrops have a depth clearly exceeding 20 m, which allowed us to gather stratigraphic information of deeper units (i.e. below basal tills) and to make statements on i) the depth range of LGM sediments and ii) the existence of pre-LGM sediments of prior glacial maxima (i.e. PGM). Sand sized intercalations of hour distinct fluvial units were sampled for luminescence dating and verified by considering the morphostratigraphic context (i.e. of LGM landforms). Lithofacies in outcrops are defined according to their dominant grain size class, texture, fabric, stratification, degree of clast rounding, and sorting. The lithofacies description in this study uses a slightly modified coding system from Keller (1996) and Heinz et al. (2003) which are based on the concept introduced by Miall (1978) and Eyles et al. (1983) (see Table 1 for classes). Vertical positions in outcrops were determined using a terrestrial laserscan model. Data were acquired from several scan positions and merged into a common coordinate system using tiepoint positions (reflectors) based on a differential-GPS. Applied postprocessing steps comprise the homogenization of point density, the elimination of erroneous data (terrain filtering), and the triangulation of the data to a closed surface mesh.

Table 1
Lithofacies codes and according description. The facies codes are slightly modified from Keller (1996) and Heinz et al. (2003) which base on the concept introduced by Miall (1978) and Eyles et al. (1983).

Lithofacies code	Description
cGmm	Gravels with cobbles, matrix-supported, massive (no bedding)
cGcm	Gravels with cobbles, clast-supported, massive (no bedding)
Gcg	Gravels, clast-supported, graded
Gcg, a	Gravels, clast-supported, graded, alternating (bimodal with open-framework)
Gch	Gravels, clast-supported, horizontally stratified
Gcp	Gravels, clast-supported, planar stratified
Gct	Gravels, clast-supported, trough cross-stratified
Dmm	Diamict, matrix-supported, massive
Sm	Sand, massive
St	Sand, trough cross-stratified
Sh	Sand, laminated horizontally
sFm	Fines with sand, massive
Fl	Fines, laminated

3.2. Well log assessment, DEM data

Most drillings (several hundreds), which were taken to analyze the Quaternary strata, were encountered for the purpose of coal exploration (~90%). Some additional logs come from drillings done for the installation of water gauging stations or to implement explosives for seismic surveys (for hydrocarbon exploration). Drillings for coal exploration base on the counter flush drilling mode which allow accurate determination of depth and thickness of layers (in the order of centimeters, e.g. Brix and Schulz, 1993). Log description base on cores and cuttings (diameters ~ 2–3 cm) which brought by the flush from the base (i.e. the drill tube) to the surface. Relevant log information (for this study) typically provides the main component (e.g. gravel) and the subordinate components (e.g. sand, loam). Some comments are given additionally (e.g. "hard to drill" typically associated with overconsolidated basal till). Recorded accuracy in the Miocene layers (coal bearing) can be derived from the paper logs to be in the order of few centimeters. The record of fine (cm-thick) changes in the coarse-grained Quaternary strata is potentially limited in the log-data (no primary target) but they do well record striking features which are of main interest in this study. These include the Quaternary/Neogene unconformity and clear changes in the sedimentary column exceeding some decimeters in thickness (changes in the main component, for example intercalations of basal till).

Topographic information comes from high-resolution DEMs (airborne-LiDAR) which have a ground resolution of 1 m. For more details on the original data and processing see Salcher et al. (2010).

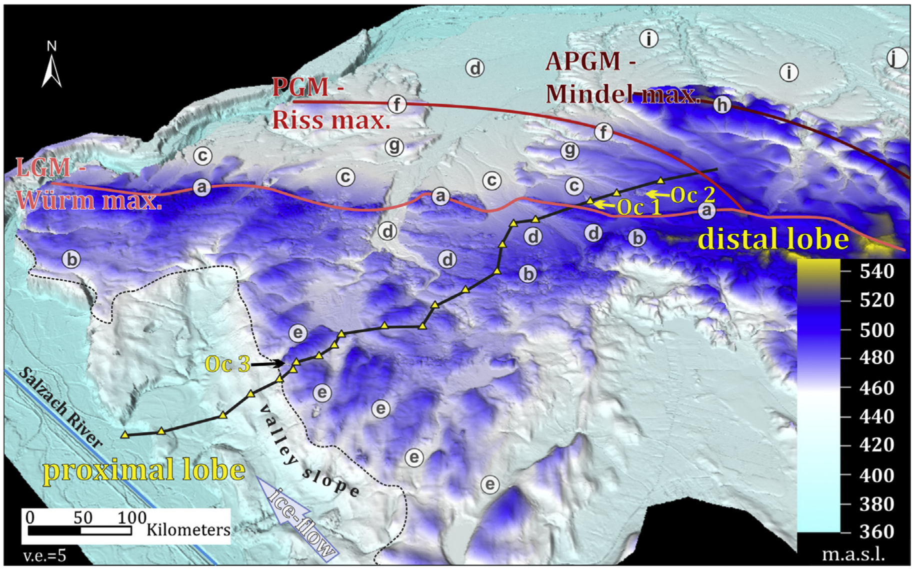

Fig. 2. Oblique view of Salzach glacier's terminal lobe part. The black line marks the position of the cross section (Fig. 11) with yellow triangles showing the position of the analyzed drillings. "Oc" indicates outcrop 1, 2 and 3. Dashed line marks the transition of the valley slope to the preserved glacial landforms (dark blue). Letters indicate prominent landforms on top of the plateau according to Salcher et al. (2010). **a**: LGM (Würm full-glacial period) terminal moraine 1; **b**: LGM terminal moraine 2; **c**: LGM, upper outwash with sub-terrace levels; **d**: LGM, lower outwash with sub-terrace levels; **e**: tunnel channels of subglacial drainage system (LGM); **f**: PGM (Riss maximum) terminal moraine 1; **g**: PGM terminal moraine 2; **h** and **i**: APGM (Mindel maximum) terminal moraine and outwash; **j**: terminal moraine of the earliest glacial maximum (preantepenultimate, "Günz"). DEM resolution is 10 m (resampled from airborne LiDAR, for details see Salcher et al., 2010). (For interpretation of the references to colour in this figure legend, the reader is referred to the web version of this article.)

3.3. Luminescence dating

Luminescence dating is based on the effect of ionising radiation causing defect in the crystal lattice of mineral grains. These defects accumulate over time and can be removed by heating or illumination. If this happens, a certain amount of energy, the luminescence signal, is released and quantified as equivalent dose (D_e). Provided a constant known rate of incoming ionizing radiation (dose rate), the time elapsed since a mineral grain was last exposed to sunlight can be calculated (Aitken, 1998; Preusser et al., 2008). For dating of quartz, we took four sediment samples by hammering stainless steel tubes (15 cm long, 4 cm in diameter) into freshly cleaned outcrops of fluvial sediments (n = 4, two in Outcrop 1 and Outcrop 3, respectively, see below for details on sediments). All further analysis steps were carried out in the laboratory under subdued red-light conditions. The outermost, light-exposed parts of the samples were removed before chemical treatment with hydrochloric acid (10 vol%) and hydrogen peroxide (10 vol%) to get rid of carbonates and organic content, respectively. After every treatment step, samples were washed with distilled water. The 180–212 μm sand fraction was prepared by dry sieving and density separation using heavy liquid (LST Fastfloat, 2.62 g/cm^3). The quartz separates were then etched with 40 vol% HF for 40 min in order to remove the outer ~20 μm mineral layer affected by alpha irradiation. Then they were treated with HCl (30 vol%) and rinsed with water. Re-sieving ensured that all the grains etched to a diameter <180 μm were removed. Measurement aliquots were produced by mounting the grains onto stainless steel discs (9.7 mm diameter) using silicone oil spray. While for preheat test measurements these were medium (3 mm) sized, small (2 mm) aliquots were used for dating. This means that in the latter case not more than around 100 quartz grains per aliquot were measured, of which, however, only an estimated 5–10% emit a measurable signal (Duller, 2008; Lowick et al. report even lower percentages of <0.5% from their samples in the Swiss alpine foreland). Luminescence measurements were carried out by either using a Risø TL/OSL DA-15 Reader equipped with a calibrated $^{90}Sr/^{90}Y$ beta source (~0.08 Gy^{-1}) or a Risø TL/OSL DA-20 Reader equipped with a calibrated $^{90}Sr/^{90}Y$ beta source (~0.10 Gys^{-1}). The quartz signal was stimulated using blue LEDs (470 nm) and detected through a Hoya U340 (7.5 mm) filter. For all measurements, heating was at 5°C^{s-1} in a nitrogen atmosphere. A measurement error of 1.6% was derived experimentally and assumed for all equivalent dose (D_e) estimations. Coarse-grained quartz samples were measured using the single aliquot regenerative dose (SAR) protocol (Murray and Wintle, 2000, 2003) including a check for feldspar contamination (IR-OSL depletion ratio after Duller, 2003). Preheat plateau tests were performed, showing stable L_x/T_x values over the temperature range 220–280 °C. Preheat for all following measurements was held at 240 or 260 °C for 40 s, and cut heat (0 s) was set at temperatures 20 °C lower than the previous preheat of the respective sample. A single saturation exponential function was plotted to fit the regeneration dose points, and D_e values were calculated using the first 0.3 s of the decay curve, with a background subtraction of the last 10 s. For the dating sequences, the following rejection criteria were applied: (i) the detected signal had to be more than three times the background; (ii) recycling ratio had to be within 0.9–1.1; (iii) recuperation had to be below 5%; (iv) maximum test dose error had to be 10%. All samples were tested to see whether the chosen protocol was able to recover a known laboratory dose administered to previously light-exposed and unheated sediment samples. This dose recovery test (Murray and Wintle, 2003) is an important check for the suitability of the material for luminescence dating and ideally yields a measured/given dose ratio close to unity. After the samples were bleached by exposing them to natural sunlight, they were given laboratory beta doses similar tor their natural D_e values (PFA 1: 30 Gy; PFA 3: 208 Gy; Doe1: 323Gy; Doe2: 323 Gy).

The dose rate consists of contributions from alpha, beta, gamma and cosmic radiation plus a small alpha and beta dose from radioactive inclusions inside the grains. For determination of the external dose rate, thick source alpha (on a Daybreak 583 alpha counter) and beta counting (on a Risø GM25-5 beta counter) was used to obtain concentrations of uranium, thorium and potassium. Alpha, beta and gamma dose rates were then calculated using the conversion factors provided by Adamiec and Aitken (1998). Beta attenuation values were taken from Aitken (1998) and a mean a-value of 0.04 ± 0.002 Gy/ka was used (Rees-Jones, 1995). Cosmic dose rate values were obtained using the equations given by Prescott and Hutton (1994). To make sure that the dose rate calculations are not biased by in-homogeneity of the gamma radiation emitted by the sediment around the respective sampling spot, field gamma spectrometry using an Ortec NaI Scintillation Detector was carried out. Present-day water content values were determined after drying the sediment samples at 100 °C for 24 h. The values range between 1 and 8% and are considered as minimum values. Therefore, a water content of 15 ± 10% was chosen for age calculations, ranging from almost dry to nearly saturated conditions (Bickel et al., 2015). Relevant data are presented in Table 2. The software ADELE (Kulig, 2005) was used for age calculations.

4.1.2. Channel facies

The channel facies is characterized by better sorting and structure than the sheetflood facies (Fig. 5) typical reflecting deposits of a gravel braided-river. Clast-supported, medium gravels to cobbles with a matrix of medium to coarse sands dominate. Clasts are rounded to well-rounded. Bedding is (sub-) horizontal (cGch) (Fig. 5b) to cross-stratified. Horizontal bed boundaries are vague and single beds have thicknesses of some cm to few decimeters. Cross-stratification is related to planar bedding (Gcp) (Fig. 5c) and trough cross-stratified bedding (Gct) (Fig. 5b). Channels have common depths of some decimeters and horizontally extensions of few meters to some tens of meters. Aside from cross-stratified gravels, channel fills also include cross-stratified sands (St) (Fig. 5b, d) and clast-supported massive gravels without clear stratification (Gcm). Gravel-couplets with some cm thick alternations of normally graded open framework gravels and bimodal sandy gravels (Gcg, a) can be also occasionally recognized (Fig. 5b).

Table 2

Names and geographic positions of the sites visited for luminescence dating, with sample codes, depth below surface, water content [WC], concentrations of dose-relevant elements and resulting dose rates.

Site	Sample code	Elevation (m a.s.l.)	Sample depth (m)	WC [%]	U [ppm]	Th [ppm]	K [%]	DR_{Qu} (Gy ka^{-1})
Outcrop 1 (48°06′17″N/12°55′54″E)	PFA1	474	7	15	1.32 ± 0.05	3.54 ± 0.16	0.56 ± 0.03	1.0 ± 0.2
	PFA3	471	11	15	1.26 ± 0.04	1.98 ± 0.13	0.84 ± 0.07	1.1 ± 0.2
Outcrop 3 (48°03′41″N, 12°50′44″E)	Doe1	465	17	15	1.41 ± 0.04	3.61 ± 0.15	0.84 ± 0.03	1.4 ± 0.2
	Doe2	472	24	15	1.52 ± 0.07	6.66 ± 0.23	0.76 ± 0.04	1.6 ± 0.2

4. Results

4.1. Lithofacies in analyzed outcrops

Three major facies of glacial- and glaciofluvial sediments dominate the analyzed outcrops (Table 1, Fig. 3; see chapter 3.1. for applied lithofacies scheme): (i) the sheetflood facies (Gcm-cGmm) in Outcrop 1 and 2, representing the distal parts of the SGL, (ii) the channel facies in Outcrop 3 representing the proximal parts of the SGL and (iii) the basal till found in Outcrop 1 and 3.

4.1.1. Sheetflood facies

This lithofacies association is dominated by crudely horizontally bedded coarse grained massive to clast-supported gravels with cobbles (cGmm-cGcm) (Fig. 4b, unit A). Outsized sub-angular to sub-rounded clasts up to boulder size do occasionally occur but appear isolated, “floating” in the sediment. Rounding of these large clasts is general poor (sub-angular to sub-rounded) and clearly lower compared to the gravel-sized fraction (rounded to well rounded). Beds have thicknesses of several centimeters to few decimeters and common lengths of some tens of meters. Crudely developed normal grading (Gcg) associated with an increase in matrix content can occasionally be observed. The gravel beds are occasionally topped by thin, several cm thick, and up to few tens of meters wide sheet-like lenses of massive sand (Sm) (Fig. 4b). These massive sand layers may contain an admixture of fine to medium gravels (gSm) but also a certain amount of silt. Lower bounding surface angles of these sand sheets are gently curved and gradual, covering shallow depressions, while upper boundaries are straight and sharp. Rarely, we observed sections with antidunes showing heights of some cm and wavelengths of few dm. Gravel-couplets (~10–20 cm) with a lower zone of bimodal sandy gravels and an upper zone of open-framework gravels with cobbles are also typical for the sheetflood facies (cGcg, a). However, they are rare compared to the channel facies and are hardly inclined forming horizontal to sub-horizontal layers.

Channel fills have a more distinct imbrication than observed for the horizontal beds, with clasts oriented parallel to the avalanche face. Fills may also comprise interfingering cross-beds with opposite growth directions (i.e. confluence scours, Fig. 5b).

4.1.3. Basal till facies

This facies represents a matrix supported, massive diamict (Dmm), which is overconsolidated (Fig. 4g, h; Fig. 5e, g). The sediment appears commonly brown to yellowish colored and structureless but may also show thin (cm-thick) layers of deformed massive fines (Fm) sometimes with vague foliation. Rounding covers the whole range with clasts dominated by rounded to subangular components. Striation of clasts is very common (Fig. 5g) and cracked clasts are sometimes observed (Fig. 5h). Glacitectonic features such as deformed fines may also occur. Horizontally laminated fines (Fl) on top of these diamicts are rare, showing a thickness of only few cm (Fig. 4h, i) and a similar color as the diamict. Individual laminae are about 1–2 mm thick. Drill logs commonly recognize the basal till facies as loam with gravels and/or sands.

4.2. Stratigraphy at distal SGL positions (outcrop 1, 2)

Outcrop 1 is situated within fluvial outwash associated with the terminal moraine representing the most extensive advance of the Salzach glacier during the LGM (Figs. 2 and 6). Glacial landforms of the PGM are situated directly north of it. The outcrop has a maximum depth of ~30 m showing a succession of three coarse grained, massive units all dominated by the sheetflood facies with only slight variations in structure: The upper sheetflood unit appears completely unweathered (Fig. 4a, b) with a thickness varying from ~15 m in the southern part of the outcrop to only 4 m in the northern part. Thinning is largely related to the slope of the outwash (fan) of more than 1° declining from the terminal moraine at ~485 m a.s.l. to the edge of the outcrop at ~476 m.a.s.l. The erosional lower surface of the upper unit appears as a clear unconformity (Fig. 4a, d, e). We processed sediment for luminescence

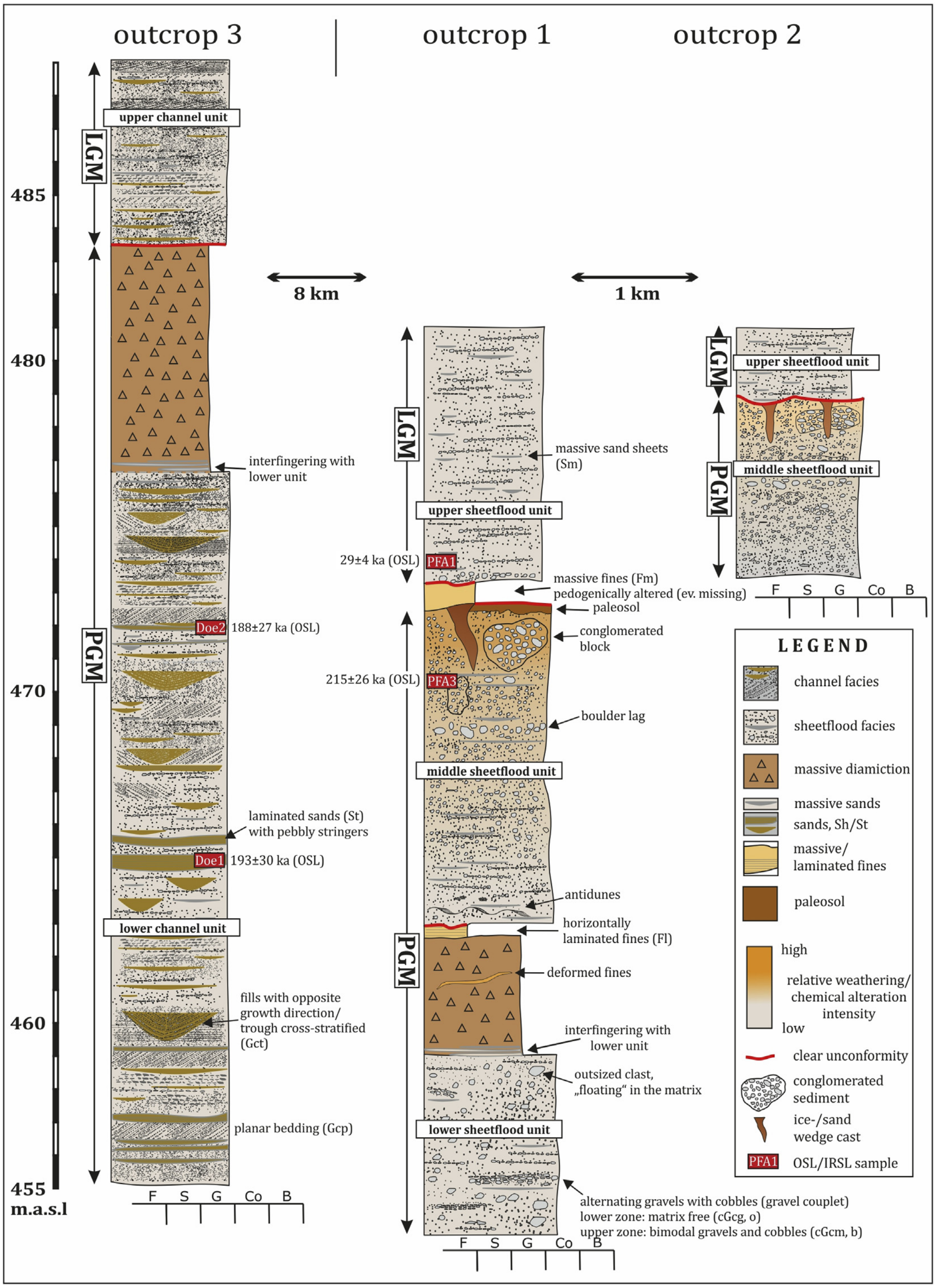

Fig. 3. Geological profiles of outcrops 1 and 2 representing deposits of the distal SGL position and of outcrop 3 representing deposits of the proximal SGL position. Features in the profiles indicate the main sedimentary structures of each facies (not to scale). See text for details on age interpretation.

dating near the base of this upper unit, from an about 12 cm thick and an about 4 m wide sandy channel fill (Sm). The OSL age was 29 ± 4 ka (Fig. 3; Table 3). The upper sheetflood unit is separated by a sharp unconformity from the middle sheetflood unit (~8–10 m). The top few decimeters appear altered into a brown to dark red paleosol associated with increased content of matrix and chemically altered gravel clasts (Fig. 4e, f). Crystalline clasts are often disaggregated and carbonates are dissolved into a loose, pulverulent consistence. This paleosol may also form distinct wedge-shaped areas to ~3 m depth tapering downwards (Fig. 4e). Below the paleosol, sediment is often conglomerated into distinct blocks with diameters to ~3 m. Right below this weathered zone we processed a second sample for OSL dating. An about 15 cm thick lenticular-shaped sandy channel fill of this middle sheetflood unit was dated to 215 ± 26 ka (Fig. 3; Table 3). In some parts, the upper and the middle sheetflood unit are separated by an up to only 0.3 m

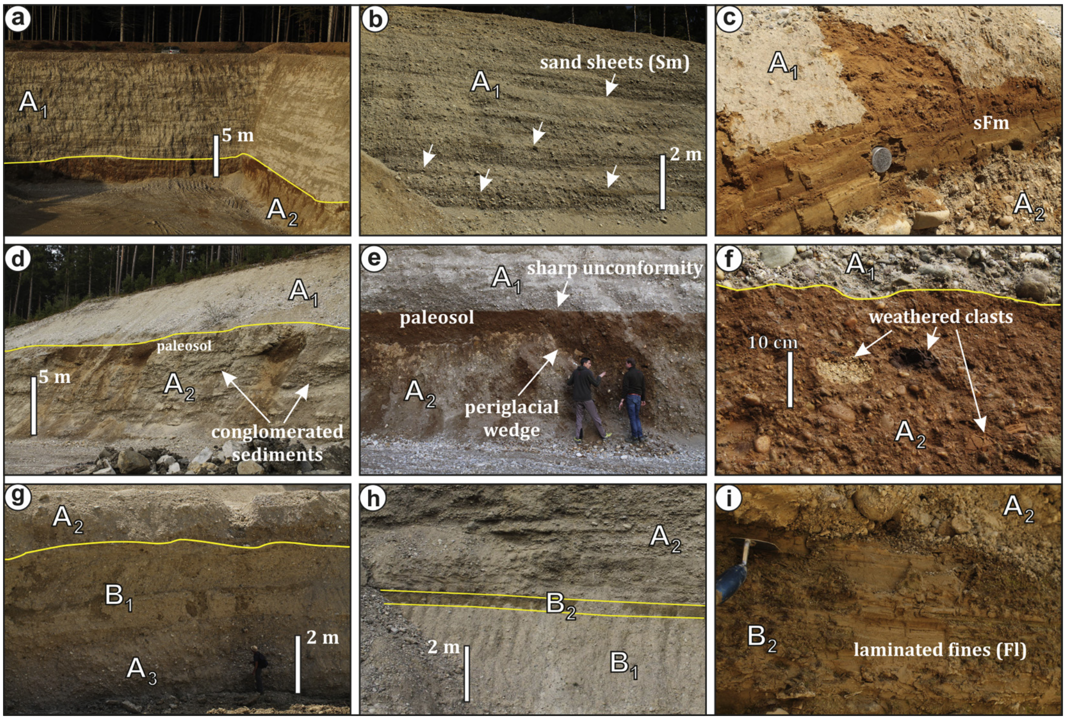

Fig. 4. Sedimentary structures in outcrop 1. A_1: upper sheetflood facies, A_2: middle sheetflood facies, A_3: lower sheetflood facies. B_1: basal till facies. B_2: Laminated fines on top of massive diamicts. Lines indicate unconformities. For details on lithofacies see text, for details on stratigraphy see Fig. 7. For position of outcrops see Fig. 2.

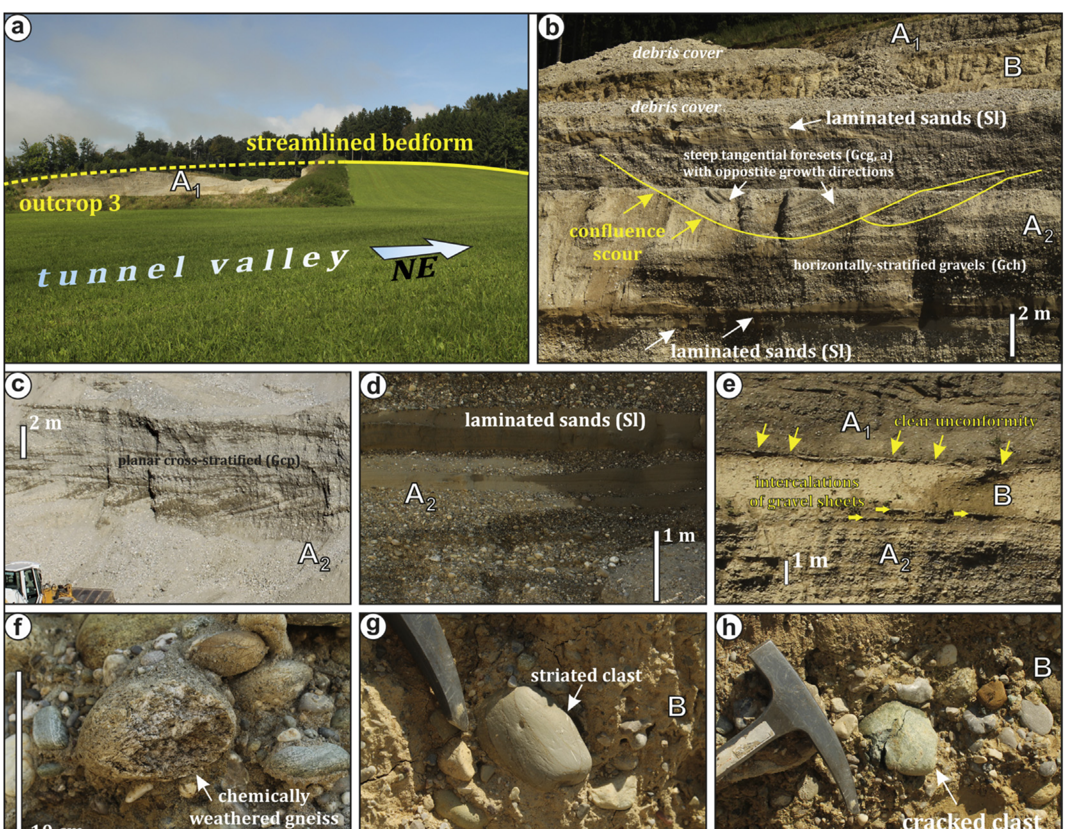

Fig. 5. Geomorphology and sedimentary structures in outcrop 3. A_1: upper channel facies, A_2: lower channel facies. B: basal till facies. A_1 and A_2 are separated by B. For details on lithofacies see text, for details on stratigraphy see Fig. 7. For position of outcrops see Fig. 2.

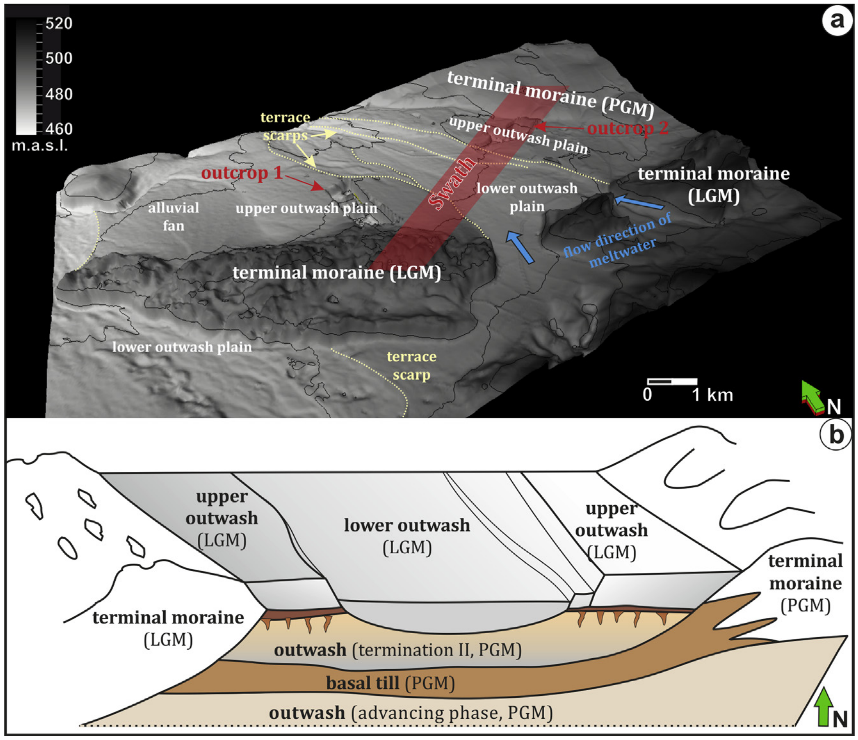

Fig. 6. a: Topography at the distal area of the SGL, between LGM and PGM terminal moraines. Outcrop 1 and 2 are situated in outwash associated with the terminal moraine of the most extensive position of the LGM (terminal moraine 1; Fig. 2). Steep outwash slope and the formation of alluvial fans indicate the sedimentary environment (sheetflood facies). Lower outwash is associated with the more proximal LGM terminal moraine 2 LGM (Fig. 2). DEM resolution: 1 m. b: Sketch illustrating LGM and PGM landforms and deposits at the terminal SGL. Basal till indicates overriding of the outwash deposited in the forefield of the glacier during the advancing stage of the PGM. Later, during ice collapse (termination II), local outwash was deposited on top of the basal till. These sediments were subjected to intense soil forming processes (last interglacial) and occasionally covered by loess during an early period of the last glacial period. Soils and outwash were hardly eroded during the LGM. Note the close position of LGM and PGM extent marked by the terminal moraines. The sketch is in well accordance with Penck and Brückner's (1909) glacial series model. For details on stratigraphy see Fig. 7.

thick layer consisting of a yellowish to brownish massive coarse silt to fine sand (sFm) (Fig. 4c).

The lowest and third sheetflood unit is separated from the middle unit by a ca. 3–4 m thick layer of basal till (Fig. 4g, h) and is dominated by crudely, horizontally bedded massive gravels and cobbles (cGmm). While there is a clear unconformity between the basal till and the middle unit above, the transition between the till and the lower unit is less clear with gravel sheets intercalated into the till within the upper few meters.

Lithologic logs of three drillings encountered within the area show that the Quaternary deposits have a total thickness of about 60 m at the outcrop location. The described outwash succession representing the upper and the (weathered) middle unit can also be observed in Outcrop 2 (Figs. 2 and 6) situated 1 km east of Outcrop 1. The total depth of Outcrop 2 is lower providing a vertical view of 8–10 m, with the upper unit thinned to 2–3 m. The alteration of the top middle sheetflood unit is here less intense and the thin layer of massive silt and fine sand is generally missing.

4.3. Stratigraphy in the proximal parts of the SGL (outcrop 3)

Outcrop 3 is situated at the eastern Salzach valley slope (i.e. the Salzach tongue basin), ~8 km southwest of Outcrop 1 (Fig. 2) giving insights into the thick pile of glacial and glaciofluvial sediments (Fig. 3). These Quaternary sediments are encountered in numerous drillings unconformably resting on top of glacially eroded Miocene strata (Fig. 7). Three well distinguishable units have a total thickness of 30 m in the outcrop. The upper and the lower unit is built up by the channel facies (Fig. 5a–e) and the middle unit, separating the two, comprises the basal till facies (Fig. 5b,g,h). The thickness of the upper unit varies from the southwestern side of the outcrop (Salzach valley slope) to thicken towards the northeast, following the shape of a 1.2 km long and a 340 m wide streamlined bedform (Salcher et al., 2010) (Fig. 5a). Accordingly, the upper unit is almost absent in the very southwest end of the outcrop and shows its maximum thickness in the northeast (~15 m). The underlying basal till facies is separated by a sharp unconformity. The diamict is highly consolidated and varies in thickness from about 2 to 5 m. Similar to outcrop 1, the boundary to the underlying unit (channel facies) is not a sharp unconformity: The diamict shows some cm thick intercalations of gravel sheets within the lower few decimeters (Fig. 5e).

Striking elements of the lower channel unit are intercalations of up to some dm thick and several tens of meters long, lenticular-shaped bodies of medium to coarse sand (Fig. 5d). Upper boundaries of these sand bodies are straight or slightly undulating, the erosional lower bounding surface angles have commonly very gentle convex forms. Sands are horizontally to sub-horizontally bedded and show well-developed laminae of up to few millimeters in thickness (Sh). Laterally interfingering of pebbly stringers is common (Fig. 5d), often appearing as sand/gravel mixtures (Gmm). Two of these major sand layers (Sh) which are apart by about 7 m have been OSL dated to 188 ± 27 and to 193 ± 30 (Fig. 3; Table 3). We did not observe any clear coarsening upward trend within both channel units, underlying and overlying the basal till, respectively.

4.4. Borehole data

Almost all of the analyzed drillings fully encounter the Quaternary deposits showing a common thickness of several tens of

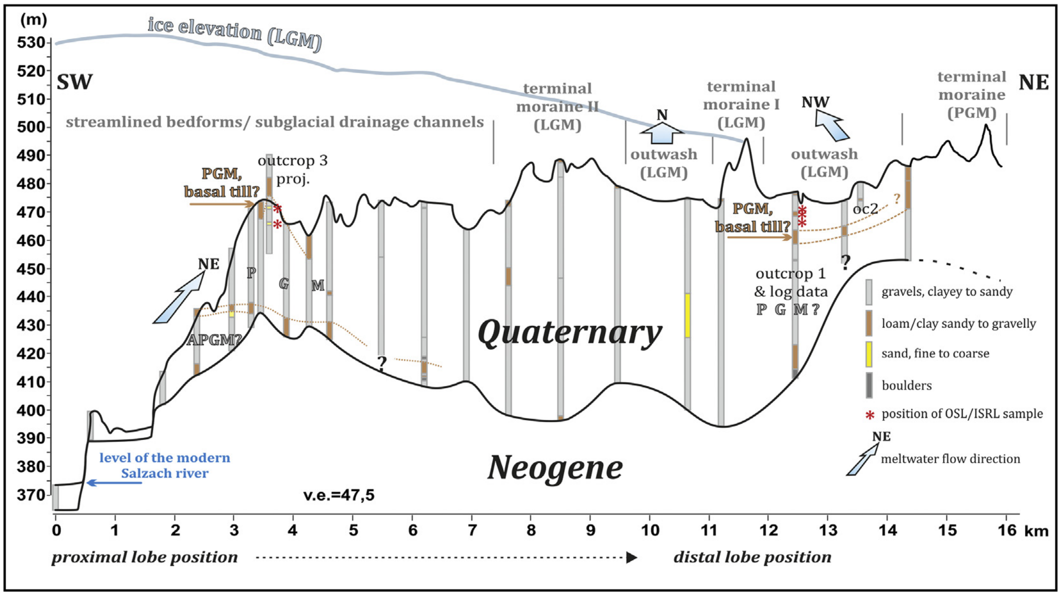

Fig. 7. Interpreted cross section through the glacial and glaciofluvial deposits of the SGL based on drill logs (see Fig. 2 for position). The shape of the Quaternary/Neogene boundary shows that glacial bedrock erosion affected the entire lobe and not only the central part. Glacial erosion during early full-glacial periods was probably followed by accumulation during the PGM and LGM. Upper black line marks the present-day topography (based on a 10 m DEM). Classification of landforms is based on Salcher et al. (2010). LGM ice elevation is based on van Husen (1987). Outcrop 3 is located in a streamlined bedform (topogr. high) and is projected to the profile (~150 m). Parts below outcrop 1 are derived from log data. Outcrop two is indicated (oc2). For location of outcrops see Fig. 2. Note: All drillings reached the Quaternary/Neogene boundary and clearly encountered the Miocene. Neogene strata (mostly fine clastics) omitted for clarity.

meters in the study area (Fig. 7). Well recognized changes in the sedimentary column of the Quaternary are decimeter to meters thick fine clastic deposits described as loam with gravels and sands (till). These deposits are typically intercalated in the glaciofluvial sediment described as coarse gravels with a sandy to clayey matrix. The Neogene sediments commonly comprise fine clastic sedimentary units with coal bearing layers ("Upper Freshwater Molasse" e.g. Weber and Weiß, 1983; Kuhlemann and Kempf, 2002) (not depicted in the profiles, Fig. 7). Gravel deposits of up to few meters thickness maximum may occasionally occur on top of these fines (Aberer, 1957; Weber and Weiß, 1983). These Neogene gravel clasts are generally clearly smaller, better sorted than those of the Quaternary and are exclusively built up by vein quartz and metamorphic basement rocks (Aberer, 1957; Weber and Weiß, 1983). The clear difference in lithofacies and change in provenance make an explicit determination between Quaternary and Neogene strata very easy to detect and straightforward. In the axis of the former glacier lobe, the modern Salzach River appears deeply incised into Quaternary and Neogene sediments (Fig. 7). Towards east and northeast, the thickness of the Quaternary deposits strongly increases as a function of the lower gradient of the underlying top Miocene compared to the higher gradient of the surface (Fig. 7 between 1,5-3,5 km). The top Neogene reaches a gentle high (~430 m a.s.l.) just below the highest position of the modern valley slope face (~480 m a.s.l.). To the east, top Neogene appears as an undulating surface with a wavelength of few kilometers and amplitudes of few tens of meters.

4.5. Luminescence dating

Fig. 8 shows representative dose response and decay (inset) curves for quartz samples which passed the rejection criteria and were used for dating in our study. They show an OSL signal strongly dominated by the fast component and are sufficiently bright. $2D_0$ values, which represent 85% of the signal saturation (Wintle and Murray, 2006) are around 300 Gy for quartz. Because of this, reliable ages back to around 300 ka should generally be expected when dose rates are around 1. However, the natural D_e in our four samples yielded values clearly lower than this (see Table 3), indicating that for none of our samples the signal is saturated. While for sample PFA1 the dose recovery test yielded a perfect match between measured and given dose, the respective results for the other samples are within ±10% of unity (Fig. 9). These results show that the OSL-SAR protocol as outlined above is able to yield reliable D_e values for the respective samples.

Table 3
Results from quartz-OSL measurements from samples collected at the Pfaffinger (PFA1, PFA3) and Doestling (Doe1, Doe2) sites, with aliquot numbers (n) used for dating, central age model (CAM) equivalent doses (De), overdispersion (OD) and calculated ages.

Outc. Nr.	Sample code	Quartz			
		n	CAM D_e (Gy)	OD (%)	Age (ka)
1	PFA1	14	28.9 ± 2.0	11.6 ± 1.3	29 ± 4
1	PFA3	14	242.5 ± 9.3	10.3 ± 1.1	215 ± 26
2	Doe1	16	238.9 ± 27.5	45.1 ± 5.6	193 ± 30
2	Doe2	14	249.9 ± 23.5	34.3 ± 4.0	188 ± 27

5. Discussion

5.1. Luminescence data

The 2 D_0 vales presented from quartz sand samples in this study are in agreement with other data from the Northern Alpine Foreland like e.g. recently presented by Bickel et al. (2015) and Lowick et al. (2015). The latter, however, reporting a large scatter from 200 to 600 Gy for quartz. The D_e values in our present dataset are all clearly lower than the respective 2 D_0 values (see Table 3) and can therefore be used for age calculations. Although the OSL signal from alpine quartz samples is known to rapidly deplete to zero within minutes under ideal conditions (e.g. Starnberger et al., 2013a),

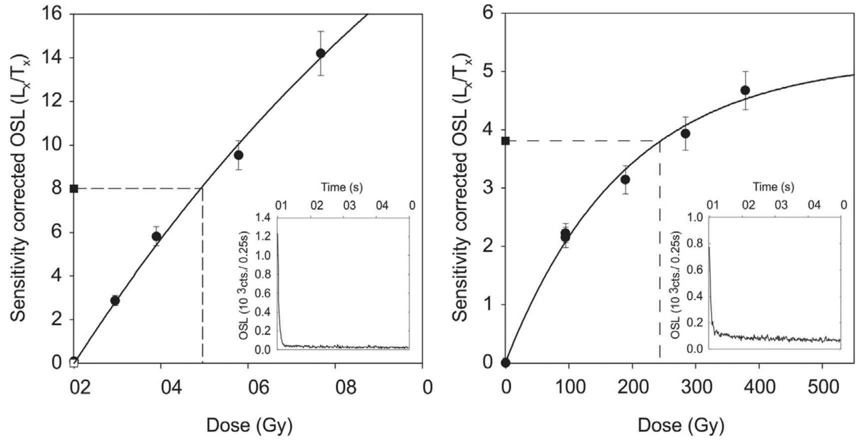

Fig. 8. Typical regeneration dose response and natural signal decay (insets) curves for the quartz-OSL signal of samples PFA1 (left) and PFA3 (right), both from outcrop 1.

fluvial and especially glacio-fluvial samples are commonly affected by partial bleaching. We decided to use small measurement aliquots (2 mm) where only 100 or less sand grains are measured, in order to reduce large signal averaging effects. The scatter in D_e values is then a good approximation to the actual variability in the degree of bleaching of the sediment. We display all the measured D_e values in Abanico plots (see Galbraith and Green, 1990; Dietze et al., 2014 for more details) which are a combination of the classical radial plot and a kernel density estimation (KDE) plot. Table 3 gives and additional overview of sample codes, overdispersion (OD) values and calculated ages based on the central age model (CAM). OD is below 20% for the samples from outcrop 1, which indicates relatively good bleaching of these samples. Distinctively higher OD values, however, were yielded for samples from outcrop 3, pointing at poor bleaching properties. These observations are supported by the KDE plots in Fig. 10, where the Doe1 and Doe2 samples show a broader range in distribution than PFA1 and PFA2, again indicating better bleaching of the latter samples. Better bleaching characteristics are however surprising when considering the morphostratigraphic and lithostratigraphic implications. These suggest only minor transport due to the proximity of the ice margin of the last and penultimate glaciation, respectively. This is in accordance with the observed steep outwash related to the former LGM ice margin (Fig. 6a; e.g. alluvial fans), indicating transport distances in the order of some 100 m only.

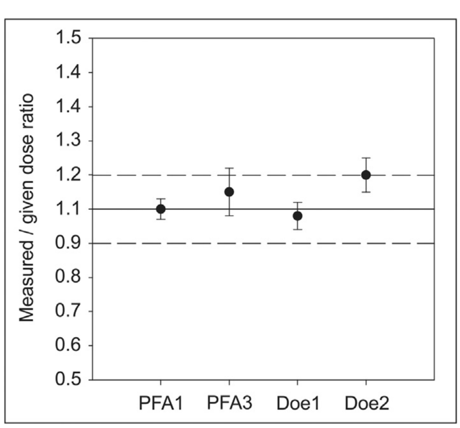

Fig. 9. Dose recovery test results for coarse-grained samples PFA1, PFA3, Doe1 and Doe2. Each data point is the result of three aliquots.

Considering the age uncertainty, the luminescence age from the upper sheetflood unit in outcrop 1 (PFA1) well fits the timing of the alpine (e.g. Ivy-Ochs et al., 2004; Monegato et al., 2007) and global LGM (26.5–20/19 ka according to Clark et al., 2009). They are also in a good agreement with prominent loess deposits some kilometers north of the SGL constraining the maximum cold period between c. 21 ± 3 and 26 ± 2 ka (Starnberger et al., 2009, 2011). The other three absolute ages from both outcrops (Doe1, Doe2, PFA3) confirm pre-LGM deposition probably during the former glaciation (MIS 6). They are in agreement with other very recent studies on the MIS 6 of the North Alpine Foreland ranging around 130 to 180 ka (Bickel et al., 2015; Lowick et al., 2015; Schielein et al., 2015). Ages may however, too old to fit the timing of the maximum cold period (PGM) rather at the end of the MIS 6 (e.g. Bard et al., 2002; Roucoux et al., 2011; Regattieri et al., 2014). A coincidence between the maximum cold period and the maximum extend of the Riss glacier (as clearly demonstrated from the terminal moraines) seems likely and is also well documented for the LGM (e.g. Ivy-Ochs et al., 2008).

A relatively large number of aliquots did not meet the rejection criteria as described above, mainly because of bad recycling ratio and/or high recuperation rates. Consequently, rejection rates for Samples PFA1, Doe1 and Doe2 were between 60 and 70%. For sample PFA3, however, the rate was smaller (44%). On the other hand, Bickel et al. (2015) had to reject even more (>80%) of their aliquots from similar alpine foreland samples. In our case, modifying the rejection criteria, e.g. accepting recuperation values below 10%, like Lowick et al. (2015) did, would increase the number of accepted aliquots, but decrease the quality of the data set.

5.2. Dynamics at the distal SGL

The three distinct gravel bed units in Outcrop 1 are interpreted to reflect high-energy, supercritical sheetflows. These non-channelized horizontal sheets are considered to represent deposits of shallow flash floods associated with the upper flow regime (Miall, 1977; Todd, 1989; Blair and McPherson, 1994). These supercritical sheetfloods are typical for building up the slopes of alluvial fans (Nemec and Postma, 1993; Blair and Mcpherson, 1994) or similar features associated with a glacier, such as ice contact fans or ramps (Benn and Evens, 1998; Krzyszkowski and Zieliński, 2002). Bed-load sheets are transferred as "waves" (Ashmore, 1991) resulting from distinct pulses of meltwater, which are also a function of the strong seasonal variations in the ablation rate of the glacier (Pisarska-Jamroży, 2006). Large floating components (cobbles and boulders) are also typical for supercritical sheet flows

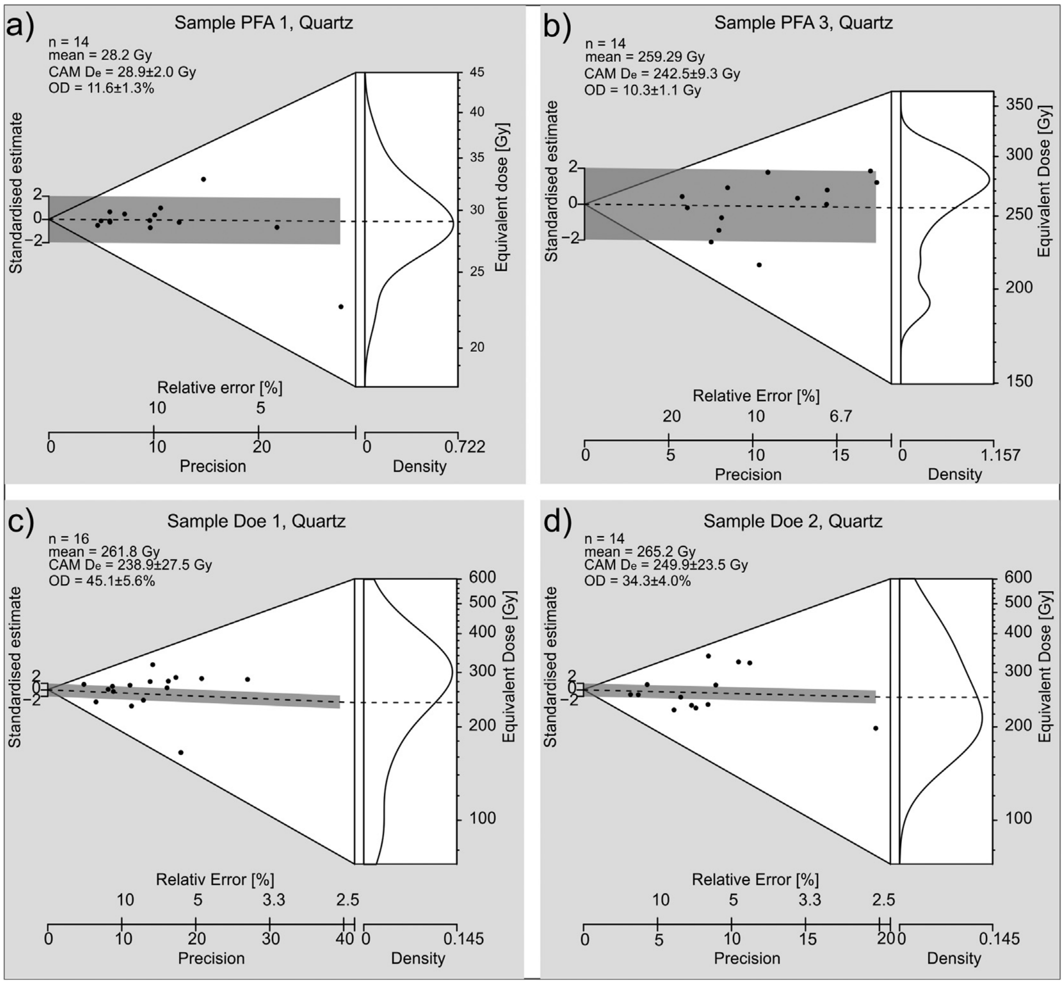

Fig. 10. Luminescence characteristics of all aliquots used for dating of coarse-grained samples from the SGL region. Abanico plots (a–d) are a combination of a radial plot and a kernel density estimate (KDE) plot (see Galbraith and Green, 1990).

(Maizels, 1997). The steep outwash slope of the upper sheetflood unit is geomorphically well expressed (Fig. 6a), supporting the ephemeral, sheet flood character (c.f Maizels, 1993). From a morphostratigraphic point of view the upper sheetflood unit must represent the LGM as it is clearly part of the "upper outwash plain" associated with the according terminal moraine of the LGM (Fig. 6; Salcher et al., 2010).

Heavily weathered and pedogenic altered material of the first few meters of the underlying middle sheet flood unit suggests ages which are clearly older than the LGM. Altered sediments are well preserved as they (i) were not overridden by the subsequent (LGM) glacier and (ii) were hardly eroded by the associated meltwaters and sheetfloods. The derived absolute age (Fig. 3) confirm pre-LGM deposition suggesting sedimentation during the former glaciation (MIS 6). From a stratigraphical point of view, the intense soil forming processes of the top middle sheetflood unit (Fig. 4e, f) must have happened during the period between termination II and the deposition of the thin loamy sequence on top (no reliable age information available due to a lack in Quartz). Consequently, soils must have been predominantly formed during the last interglacial period (MIS 5e). The grain size distribution of the loamy suggests the accumulation of loess. Later, probably with the onset of the last glacial period, permafrost conditions led to the formation of ice- or sand wedges (Fig. 4e).

Absolute age information is missing below the middle sheetflood unit. An age constraint can therefore only be relative and may derived from stratigraphic and geomorphic associations. The basal till cannot correspond to the LGM as the associated glacier did just not reach the position of the outcrop (Fig. 2). The outcrop is however within the former maximum extent of the PGM glacier (Fig. 2) directly south of the PGM's terminal moraine. A till age older than the PGM is unlikely (e,g. Mindel/APGM) as the consequence would be either no erosion provided by the PGM glacier or at least an unknown amount just leaving the basal till uneroded. It would furthermore mean that the PGM glacier did not accumulate basal till. In turn, a PGM age of the basal till well fits into Penck and Brückner's model of the "glacial series" (Fig. 6b; Penck and Brückner, 1909).

In accordance we interpret basal till's overlying middle sheetflood unit to represent outwash during PGM glacier's downwasting phase producing the recognized unconformity (Fig. 3). The formation of glaciofluvial sediments and ice wastage deposits near former ice margins is recognized to be very common during ice wastage of termination I (i.e. kame terraces; Salcher et al., 2010). The deposition of laminated fines on top of the basal till (Fig. 3; Fig. 4i) could point to ice bed uncoupling as a function of decreasing ice overburden and meltwater pressure. The associated drop in flow velocity would then give rise to suspension sedimentation

(Clerc et al., 2012). Stagnant or slowly moving ice near the lobe terminus might also have promoted the preservation in the first place. The intercalations of gravel sheets of the lower sheet flood unit into basal till on top refer to a chronologic relation. In accordance we also tend to attribute the lower sheetflood unit to the PGM possibly representing outwash deposited during the advancing stage of the SGL (similar to the situation observed in outcrop 3).

5.3. Dynamics at the proximal SGL

The thick pile of Quaternary fluvial sediments outcropped along the Salzach valley (outcrop 3, upper and lower channel unit) shows a much better sorting and a lack of fines (low suspension load) compared to the sheetflood facies found in the distal SGL (Outcrop 1 and 2). This indicates deposition by a larger stream where higher flow depths provide higher bedforms and a more effective sorting (e.g. Todd, 1989; Lunt and Bridge, 2007). The horizontal to subhorizontal bedload sheets are interpreted to have formed just above the threshold of gravel motion while the cross-bedded strata refers to the higher discharge (and water depths) which is also suggested by open-framework gravels alternating with bimodal sandy gravels (gravel-couplets; Steel and Thompson, 1983; Bridge, 2005). The thin and isolated sand drapes found in the lower channel unit (Fig. 3; Fig. 5b,d) are also interpreted as low-stage depositional elements which formed in the dune troughs during waning stages where energy of flow and associated transport capacity decreased (e.g. Lunt et al., 2004). Coarsening upward trends, as described from many proglacial deposits subsequently overridden by a glacier (e.g. Ehlers and Grube, 1983; Maizels, 1997; van Husen, 2000), were however not observed.

Luminescence ages from the lower channel unit support deposition during the penultimate glacial maximum period, although they yield ages that are slightly too old (see 5.1). Similar to the lower sheetflood/basal till association in Outcrop 1, the interfingering of the fluvial succession with the heavily consolidated basal till on top indicates that these sediments were deposited in the forefield of the advancing SGL and were later overridden by the ice, i.e. representing the early stage of the PGM. Consequently, the basal till is interpreted to represent the same age period. Heavy glacier load on top of this fluvial sequence is not only indicated by overconsolidation but also by distinctively broken clasts (normal or sub-normal to the top) that occur in the gravel and cobble sized fraction just below and within the basal till. The regional occurrence of the basal till separating both fluvial units is also supported by drill logs (Fig. 7) and descriptions of former outcrops (Weinberger, 1952). Logs recognize this very distinct lithofacies in a range of several kilometers at ~470 m a.s.l. As suggested from the outcrop, the thickness of this diamict is clearly varying and might therefore be absent in places explaining why it is not recognized in all adjacent drillings. These variations might eventually a function of local erosion trough meltwater streams. It is however not possible from log data to make reliable statements. A non-recognition of basal till as a function of insufficient accuracy during the logging process can be excluded considering the applied drilling technique (counter-flush; Brix and Schulz, 1993) and the feasible accuracy shown in the associated log data (Weber and Weiß, 1983).

Even though no absolute ages are available from the upper unit, a clearly younger age is suggested from the lower weathering intensity of clasts compared to the PGM sediments as well as from a sharp unconformity (Fig. 5e). As coarse-grained fluvial accumulation far above the modern trunk stream is generally restricted to ice shield presence (i.e. the period of a glacial maximum, see Fig. 11c), the upper sequence is interpreted to represent the subsequent (LGM) outwash deposited during the advancing stage of the SGL. If the upper channel unit would not represent the LGM, it (and the basal till) must be related to PGM as well. This would either imply that fluvial deposition did (locally) not occur during the LGM or that it was subsequently eroded. Considering the location within a subglacial tunnel valley system which provided the important pathways for the outwash accumulation in front of the terminal moraine (Salcher et al., 2010, Figs. 2 and 5a) this scenario might

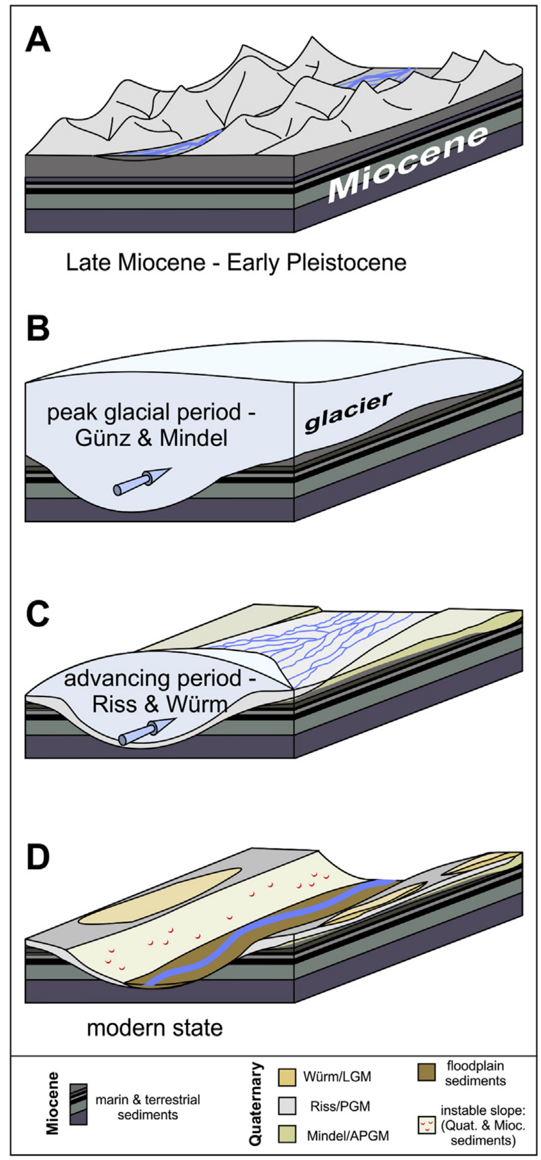

Fig. 11. Sketches illustrate the potential landscape evolution at the area of the SGL since the Late Miocene. An accumulation during several glacial maxima followed the major erosion of an initial glaciation (e.g. "Günz" sensu Penk and Brückner, 1909). A: Relief of the Miocene Molasse before the onset of glaciations affecting the North Alpine Foreland. B: After the Mid-Pleistocene transition early glaciations reached far into the North Alpine Foreland fundamentally eroding and overdeepening the Miocene bedrock. An associated effect was the sustainable deepening of the local base level. C: During subsequent glacial maxima, outwash in the forefront of the advancing glacier fills up the deepened valley. During progressive ice advances glaciofluvial sediments are overridden by the glacier. D: At the end of the glacial cycle and the collapse of the ice shield, the associated trunk stream quickly incises into the soft sediments generating slopes close to the threshold of repose. The annotations "Würm", "Riss", "Mindel" and "Günz" refer here to the glacial maxima of the last (LGM), the penultimate (PGM), the antepenultimate (APGM) and the preantepenultimate glacial maximum in the region.

rather be unlikely. In turn, the abundant meltwater discharge might however have impeded the accumulation of till on top (e.g. Cofaigh, 1996; van der Meer et al., 2003). Basal till on top is lacking but not completely absent (Weinberger, 1952).

Occurrence of basal till of stratigraphically deeper units is suggested by various drill logs at a depth of ~420–430 m a.s.l. (Fig. 7) and outcrop data (Weinberger, 1952). We suggest an analogue succession as described before, with glaciofluvial sedimentation in the glacier forefield subsequently overridden by the ice and capped by basal till (Ehlers and Grube, 1983; van Husen, 2000). This couplet of glaciofluvial sediments and basal till would then refer to one glacial maximum earlier. If true, this succession would represent the APGM ("Mindel" sensu Penk and Brückner, 1909). This view requires i) accumulation during several glacial maxima following major erosion of an initial glaciation (Fig. 11; "Günz" sensu Penk and Brückner, 1909) and ii) deposition of basal till on top of associated fluvial sediments during each glacial cycle. Major hiatuses within the Quaternary strata are, however, not indicated from outcrops and are at least locally not reported (Weinberger, 1950, 1952). Nevertheless, local erosion or the general absence of older (pre-PGM) cannot be excluded from the data. The potential role of major erosion can only be evaluated by generating further absolute ages in outcrops and/or drill cores: As sediments from glacial maxima predating the PGM (Günz and Mindel) are too old for current age estimations based on luminescence dating (Raymo, 1997), age constraints in such glaciofluvial sediments must be provided by other techniques such as cosmogenic nuclides (e.g. Akçar et al., 2014). In this context, more work on absolute chronologies in the Salzach paleoglacier region would be highly desirable.

Major erosion during an early glacial cycle is suggested by eroded Miocene deposits within the area of the SGL and the associated preserved hilly landscape just outside of the SGL's most extensive position (exceeding the Quaternary landforms by up to 250 m). Later glaciations are dominated by accumulation and carving seemed to occur only very locally as for example suggested for the "Tittmoning basin" near to the former LGM ice margin ("tongue basin"; Ziegler, 1983). With the exception of this local overdeepening, the main valley shows no further clear indication in the study area. The thin LGM deposits generally suggest that the landscape dynamics were minor compared to earlier full-glacial periods. With the end of the glacial cycle and the collapse of the SGL, the trunk river deeply cuts into the lose glaciofluvial sediments as marked for termination I by prominent terraces at different altitudes (Salcher et al., 2010). The modern Salzach River is separated by an only small, some meter thick gravel lag from the underlying Miocene.

6. Conclusions

From age determination, stratigraphy and drill log analysis, the following conclusions of the built up and dynamics of the Pleistocene SGL can be drawn:

(a) At the proximal part of the SGL, where meltwater discharge was highest during peak glacial times, the lithofacies types reflect typical deposits of a gravelly braided river. Outcrop and drill log-data indicate capping of glaciofluvial sediments by basal till deposited during the glacier's advancing stages. At the Salzach glacier this sequence development might eventually involve the LGM, PGM and APGM (Würm, Riss and Mindel full-glacial periods).

(b) The analyzed distal lobe setting seems to confirm Penck and Brückner's model of the "glacial series" showing low erosion at the lobe terminus with a typical stacked succession of (i) early stage outwash (glacier's advancing phase), (ii) basal till and (iii) late stage outwash on top (termination/end of the glacial cycle). Glaciofluvial sediments directly associated with the terminal moraine are characteristically dominated by massive sheetflood deposits. Sheetfloods are well preserved and highlight intensive soil forming processes during the last interglacial period.

(c) Deposition of thick glaciofluvial units during the Pleistocene followed intense erosion and overdeepening of Miocene bedrock which tentatively happened during early Pleistocene major glaciations in the Alpine Foreland. Luminescence ages support the observation that the majority of sediments in the study area were deposited during the PGM.

Acknowledgments

Christoph Kolmer (Government of Upper Austria) is acknowledged for providing high resolution digital elevation models and log data. Ylvie Aranmanoth's field assistance was highly appreciated.

References

Aberer, F., 1957. Die Molassezone im westlichen Oberösterreich und in Salzburg. Mitteilungen der Geologischen Gesellschaft in Wien 50, 23–94.

Adamiec, G., Aitken, M.J., 1998. Dose-rate conversion factors: update. Ancient TL 16, 37–50.

Aitken, M.J., 1998. An Introduction to Optical Dating. The Dating of Quaternary Sediments by the Use of Photon-stimulated Luminescence. Oxford University Press, Oxford.

Anselmetti, F.S., Drescher-Schneider, R., Furrer, H., Graf, H.R., Lowick, S.E., Preusser, F., Riedi, M.A., 2010. A ~180.000 year sedimentation history of a perialpine overdeepened glacial trough (Wehntal, N-Switzerland). Swiss Journal of Geosciences 103, 345–361.

Akçar, N., Ivy-Ochs, S., Alfimov, V., Claude, A., Graf, H.R., Dehnert, A., Kubik, P.W., Rahn, M., Kuhlemann, J., Schlüchter, C., 2014. The first major incision of the Swiss Deckenschotter landscape. Swiss Journal of Geosciences. http://dx.doi.org/10.1007/s00015-014-0176-6.

Ashmore, P., 1991. Channel morphology and bed load pulses in braided, gravel-bed streams. Geografiska Annaler 73, 37–52.

Benn, D.I., Evans, D.J.A., 1998. Glaciers and Glaciations. Arnold, London.

Bard, E., Antonioli, F., Silenzi, S., 2002. Sea-level during the penultimate interglacial period based on a submerged stalagmite from Argentarola Cave (Italy). Earth and Planetary Science Letters 196, 135–146.

Bickel, L., Lüthgens, C., Lomax, J., Fiebig, M., 2015. Luminescence dating of glaciofluvial deposits linked to the penultimate glaciation in the Eastern Alps. Quaternary International 357, 110–124.

Blair, T.C., Mcpherson, J.G., 1994. Alluvial fan processes and their natural distinction from rivers based on morphology, hydraulic processes, sedimentary processes, and facies s. Journal of Sedimentary Research 64A, 450–489.

Bridge, J.S., 2005. Rivers and Floodplains - Forms, Processes and Sedimentary Record. Blackwell Science Ltd, Oxford.

Brix, F., Schulz, O. (Eds.), 1993. Erdöl und Erdgas in Österreich. Museum of Natural History, Vienna.

Brückner, E., 1886. Die Vergletscherung des Salzachgebietes: nebst Beobachtungen über die Eiszeit in der Schweiz. Hölzel, Wien.

Clerc, S., Buoncristiani, J.F., Guiraud, M., Desaubliaux, G., Portier, E., 2012. Depositional model in subglacial cavities, Killiney Bay, Ireland. Interactions between sedimentation, deformation and glacial dynamics. Quaternary Science Reviews 33, 142–164.

Carlson, A.E., Mickelson, D.M., Principato, S.M., Chapel, D.M., 2005. The genesis of the northern Kettle Moraine, Wisconsin. Geomorphology 67, 265–374.

Clark, P.U., Dyke, A.S., Shakun, J.D., Carlson, A.E., Clark, J., Wohlfarth, B., Mitrovica, J.X., Hostetler, S.W., McCabe, A.M., 2009. The last glacial maximum. Science 325, 710–714.

Dehnert, A., Lowick, S.E., Preusser, F., Anselmetti, F.S., Drescher-Schneider, R., Graf, H.R., Heller, F., Horstmeyer, H., Kemna, H.A., Nowaczyk, N.R., Züger, A., Furrer, H., 2012. Evolution of an overdeepened trough in the northern Alpine Foreland at Niederweningen, Switzerland. Quaternary Science Reviews 34, 127–145.

Dietze, M., Kreutzer, S., Burow, C., Fuchs, M., Fischer, M., Schmidt, C., 2014. The art of visualising dose distributions: improved plotting flexibility for the R-package 'Luminescence'. Geophysical Research Abstracts 16.

Duller, G.A.T., 2003. Distinguishing quartz and feldspar in single grain luminescence measurements. Radiation Measurements 37, 161–165.

Duller, G.A.T., 2008. Single-grain optical dating of Quaternary sediments: why aliquot size matters in luminescence dating. Boreas 37, 589–612.

Dürst Stucki, M., Schlunegger, F., 2013. Identification of erosional mechanisms during past glaciations based on a bedrock surface model of the central European Alps. Earth and Planetary Science Letters 384, 57–70.
Ehlers, J., Grube, F., 1983. Meltwater deposits in north-west Germany. In: Ehlers, J. (Ed.), Glacial Deposits in North-west Europe. Rotterdam.
Eyles, N., Boyce, J.I., Barendregt, R.W., 1999. Hummocky moraine: sedimentary record of stagnant Laurentide Ice Sheet lobes resting on soft beds. Sedimentary Geology 123, 163–174.
Eyles, N., Eyles, C.H., Miall, A.D., 1983. Lithofacies types and vertical profile models; an alternative approach to the description and environmental interpretation of glacial diamict and diamictite sequences. Sedimentology 30, 393–410.
Farr, T.G., Kobrick, M., 2000. Shuttle Radar Topography Mission produces a wealth of data. Eos, Transactions AGU 81, 583–583.
Fiebig, M., Herbst, P., Drescher-Schneider, R., Lüthgens, C., Lomax, J., Doppler, G., 2014. Some remarks about a new last glacial record from the western Salzach foreland glacier basin (Southern Germany). Quaternary International 328–329, 107–119.
Galbraith, R., Green, P., 1990. Estimating the component ages in a finite mixture. International Journal of Radiation Applications and Instrumentation. Part D. Nuclear Tracks and Radiation Measurements 17 (3), 197–206.
Genser, J., Cloetingh, S.A.P.L., Neubauer, F., 2007. Late orogenic rebound and oblique Alpine convergence: new constraints from subsidence analysis of the Austrian Molasse basin. Global and Planetary Change 58, 214–223.
Gusterhuber, J., Dunkl, I., Hinsch, R., Linzer, H.-G., Sachsenhofer, R.F., 2012. Neogene uplift and erosion in the Alpine Foreland Basin (Upper Austria and Salzburg). Geologica Carpathia (Bratislava) 63, 295–305.
Heinz, J., Kleineidam, S., Teutsch, G., Aigner, T., 2003. Heterogeneity patterns of Quaternary glaciofluvial gravel bodies (SW-Germany): application to hydrogeology. Sedimentary Geology 158, 1–23.
Ivy-Ochs, S., Kerschner, H., Reuther, A., Preusser, F., Heine, K., Maisch, M., Kubik, P.W., Schlüchter, C., 2008. Chronology of the last glacial cycle in the European Alps. Journal of Quaternary Science 23, 559–573.
Ivy-Ochs, S., Schäfer, J., Kubik, P., Synal, H.-A., Schlüchter, C., 2004. Timing of deglaciation on the northern Alpine foreland (Switzerland). Eclogae Geologicae Helvetiae 97, 47–55.
Jennings, C.E., 2006. Terrestrial ice streams-a view from the lobe. Geomorphology 75, 100–124.
Jordan, P., 2010. Analysis of overdeepened valleys using the digital elevation model of the bedrock surface of Northern Switzerland. Swiss Journal of Geosciences 103, 375–384.
Keller, B., 1996. Lithofazies-Codes für die Klassifikation von Lockergesteinen. Mitteilungen der Schweizerischen Gesellschaft für Boden- und Felsmechanik 132, 1–8.
Kohl, H., 1998. Das Eiszeitalter in Oberösterreich Teil II: Die eiszeitliche Vergletscherung in Oberösterreich. Jahrbuch des Oberösterreichischen Musealvereines 143b, 175–390.
Krzyszkowski, D., Zielinski, T., 2002. The Pleistocene end moraine fans: controls on their sedimentation and location. Sedimentary Geology 149, 73–92.
Kuhlemann, J., 2007. Paleogeographic and paleotopographic evolution of the Swiss and Eastern Alps since the Oligocene. Global and Planetary Change 58, 224–236.
Kuhlemann, J., Kempf, O., 2002. Post-Eocene evolution of the North Alpine Foreland Basin and its response to Alpine tectonics. Sedimentary Geology 152, 45–78.
Kulig, G., 2005. Erstellung einer Auswertesoftware zur Altersbestimmung mittels Lumineszenzverfahren unter spezieller Berücksichtigung des Einflusses radioaktiver Ungleichgewichte in der 238-U-Zerfallsreihe. B.Sc. thesis. Technical University Bergakademie Freiberg.
Lowick, S.E., Buechi, M.W., Gaar, D., Graf, H.R., Preusser, F., 2015. Luminescence dating of Middle Pleistocene proglacial deposits from northern Switzerland: methodological aspects and stratigraphical conclusions. Boreas. http://dx.doi.org/10.1111/bor.12114. ISSN 0300-9483.
Lunt, I.A., Bridge, J.S., 2007. Formation and preservation of open-framework gravel strata in unidirectional flows. Sedimentology 54, 71–87.
Lunt, I.A., Bridge, J.S., Tye, R.S., 2004. A quantitative, three-dimensional depositional model of gravelly braided rivers. Sedimentology 51, 377–414.
Lüthgens, C., Böse, M., 2012. From morphostratigraphy to geochronology - on the dating of ice marginal positions. Quaternary Science Reviews 34, 26–36.
Maizels, J., 1993. Lithofacies variations within sandur deposits: the role of runoff regime, flow dynamics and sediment supply characteristics. Sedimentary Geology 85, 299–325.
Maizels, J.K., 1997. Jokulhlaup deposits in proglacial areas. Quaternary Science Reviews 16, 793–819.
Miall, A.D., 1977. A review of the braided river depositional environment. Earth Science Reviews 13, 1–62.
Miall, A.D., 1978. Lithofacies types and vertical profile models in braided river deposits: a summary. In: Miall, A.D. (Ed.), Fluvial Sedimentology. Canadian Society of Petroleum Geologists, Calgary.
Monegato, G., Ravazzi, C., Donegana, M., Pini, R., Calderoni, G., Wick, L., 2007. Evidence of a two-fold glacial advance during the last glacialmaximum in the Tagliamento end moraine system (eastern Alps). Quaternary Research 68, 284–302.
Murray, A.S., Wintle, A.G., 2000. Luminescence dating of quartz using an improved single-aliquot regenerative-dose protocol. Radiation Measurements 32, 57–73.
Murray, A.S., Wintle, A.G., 2003. The single aliquot regenerative dose protocol: potential for improvements in reliability. Radiation Measurements 37, 377–381.
Nemec, W., Postma, G., 1993. Quaternary alluvial fans in southwestern Crete: sedimentation processes and geomorphic evolution. In: Marzo, M., Puigdefabrogas, C. (Eds.), Alluvial Sedimentation: International Association of Sedimentologists. Special Publication.
Ó Cofaigh, C., 1996. Tunnel valley genesis. Progress in Physical Geography 20, 1–19.
Penck, A., Brückner, E., 1909. Die Alpen im Eiszeitalter. Tauchnitz, Leipzig.
Penck, A., 1882. Die Vergletscherung der Deutschen Alpen: ihre Ursachen, Periodische Wiederkehr und ihr Einfluss auf die Bodengestaltung. Barth, Leipzig.
Pisarska-Jamroży, M., 2006. Transitional deposits between the end moraine and outwash plain in the Pomeranian glaciomarginal zone of NW Poland: a missing component of ice-contact sedimentary models. Boreas 35, 126–141.
Prescott, J.R., Hutton, J.T., 1994. Cosmic ray contributions to dose rates for luminescence and ESR dating: large depths and long-term time variations. Radiation Measurements 23, 497–500.
Preusser, F., Degering, D., Fuchs, M., Hilgers, A., Kadereit, A., Klasen, N., Krbetschek, M., Richter, D., Spencer, J.Q.G., 2008. Luminescence dating: basics, methods and applications. EandG Quaternary Science Journal 57, 95–149.
Preusser, F., Reitner, J.M., Schlüchter, C., 2010. Distribution, geometry, age and origin of overdeepened valleys and basins in the Alps and their foreland. Swiss Journal of Geosciences 103, 407–426.
Raymo, M.E., 1997. The timing of major climate terminations. Paleoceanography 12, 577–585.
Rees-Jones, J., 1995. Optical dating of young sediments using fine-grain quartz. Ancient TL 13, 9–14.
Regattieri, E., Zanchetta, G., Drysdale, R.N., Isola, I., Hellstrom, J.C., Roncioni, A.A., 2014. A continuous stable isotope record from the penultimate glacial maximum to the Last Interglacial (159–121 ka) from Tana Che Urla Cave (Apuan Alps, central Italy). Quaternary Research 82, 450–461.
Roucoux, K.H., Tzedakis, P.C., Lawson, I.T., Margari, V., 2011. Vegetation history of the penultimate glacial period (Marine Isotope Stage 6) at Ioannina, north-west Greece. Journal of Quaternary Research 26, 616–626.
Salcher, B.C., Hinsch, R., Wagreich, M., 2010. High-resolution mapping of glacial landforms in the North Alpine Foreland, Austria. Geomorphology 122, 283–293.
Schielein, P., Schellmann, G., Lomax, J., Preusser, F., Fiebig, M., 2015. Chronostratigraphy of the Hochterassen in the lower Lech valley (North Alpine Foreland). Quaternary Science Journal 64/1, 15–29.
Starnberger, R., Rodnight, H., Spötl, C., 2013a. Luminescence dating of fine-grain lacustrine sediments from the late Pleistocene Unterangerberg site (Tyrol, Austria). Austrian Journal of Earth Sciences 106, 4–15.
Starnberger, R., Drescher-Schneider, R., Reitner, J.M., Rodnight, H., Reimer, P.J., Spötl, C., 2013b. Late Pleistocene climate change and landscape dynamics in the Eastern Alps: the inner-alpine Unterangerberg record (Austria). Quaternary Science Reviews 68, 17–42.
Starnberger, R., Rodnight, H., Spötl, C., 2011. Chronology of the last glacial maximum in the Salzach Palaeoglacier Area (Eastern Alps). Journal of Quaternary Science 26, 502–510.
Starnberger, R., Terhorst, B., Rähle, W., Peticzka, R., Haas, J.N., 2009. Palaeoecology of Quaternary periglacial environments during OIS-2 in the forefields of the Salzach Glacier (Upper Austria). Quaternary International 198, 51–61.
Steel, R.J., Thompson, D.B., 1983. Structures and textures in Triassic braided stream conglomerates ('Bunter' Pebble beds) in the Sherwood Sandstone Group, North Staffordshire, England. Sedimentology 30, 341–367.
Todd, S.P., 1989. Stream-driven, high-density gravelly traction carpets: possible deposits in the Trabeg Conglomerate Formation, SW Ireland and some theoretical considerations of their origin. Sedimentology 36, 513.
Van Der Meer, J.J.M., Menzies, J., Rose, J., 2003. Subglacial till: the deforming glacier bed. Quaternary Science Reviews 22, 1659–1685.
Van Husen, D., 1987. Die Ostalpen in den Eiszeiten. Geologische Bundesanstalt, Vienna.
Van Husen, D., 2000. Geological processes during the Quaternary. Mitteilungen der Österreichische Geologische Gesellschaft 92, 135–156.
Weber, L., Weiß, A., 1983. Bergbaugeschichte und Geologie der österreichischen Braunkohlevorkommen. Archiv für Lagerstättenforschung, 4. Geol.- B. A, Wien.
Weinberger, L., 1950. Gliederung der Altmoränen des Salzachgletschers östlich der Salzach. Zeitschrift für Gletscherkunde und Glazialgeologie 1, 176–186.
Weinberger, L., 1952. Ein Rinnensystem im Gebiete des Salzach-Gletschers. Zeitschrift für Gletscherkunde und Glazialgeologie 2.
Weinberger, L., 1957. Bau und Bildung des Ibmer Moos-Beckens. Mitteilung der Geographischen Gesellschaft in Wien 99.
Wintle, A.G., Murray, A.S., 2006. A review of quartz optically stimulated luminescence characteristics and their relevance in single-aliquot regeneration dating protocols. Radiation Measurements 41, 369–391.
Ziegler, J.H., 1983. Verbreitung und Stratigraphie des Jungpleistozäns im voralpinen Gebiet des Salzachgletschers in Bayern. Geologica Bavarica 84, 153–176.